

Article

Element Patterns of Primary Low-Magnesium Calcite from the Seafloor of the Gulf of Mexico

Huiwen Huang^{1,2,3}, Xudong Wang^{1,2,3,4,*}, Shanggui Gong⁴, Nicola Krake⁵, Daniel Birgel⁵, Jörn Peckmann⁵ , Duofu Chen^{2,4} and Dong Feng^{2,4,*} 

¹ CAS Key Laboratory of Ocean and Marginal Sea Geology, South China Sea Institute of Oceanology, Chinese Academy of Sciences, Guangzhou 510301, China; huiwenhuang@scsio.ac.cn

² Laboratory for Marine Mineral Resources, Qingdao National Laboratory for Marine Science and Technology, Qingdao 266061, China; dfchen@shou.edu.cn

³ University of Chinese Academy of Sciences, Beijing 100049, China

⁴ Shanghai Engineering Research Center of Hadal Science and Technology, College of Marine Sciences, Shanghai Ocean University, Shanghai 201306, China; sggong@shou.edu.cn

⁵ Institute for Geology, Center for Earth System Research and Sustainability, Universität Hamburg, 20146 Hamburg, Germany; nicola.krake@uni-hamburg.de (N.K.); daniel.birgel@uni-hamburg.de (D.B.); joern.peckmann@uni-hamburg.de (J.P.)

* Correspondence: xdwang@scsio.ac.cn (X.W.); dfeng@shou.edu.cn (D.F.)

Received: 12 February 2020; Accepted: 25 March 2020; Published: 27 March 2020



Abstract: High-magnesium calcite (HMC) and aragonite are metastable minerals, which tend to convert into low-magnesium calcite (LMC) and dolomite. During this process, primary compositions are frequently altered, resulting in the loss of information regarding the formation environment and the nature of fluids from which the minerals precipitated. Petrological characteristics have been used to recognize primary LMC, however, neither the element distribution within primary LMC nor the effect of diagenetic alteration on element composition have been studied in detail. Here, two mostly authigenic carbonate lithologies from the northern Gulf of Mexico dominated by primary LMC were investigated to distinguish element compositions of primary LMC from LMC resulting from diagenetic alteration. Primary LMC reveals similar or lower Sr/Ca ratios than primary HMC. The lack of covariation between Sr/Ca ratios and Mg/Ca ratios in the studied primary LMCs are unlike compositions observed for LMC resulting from diagenetic alteration. The Sr/Mn ratios and Mn contents of the primary LMCs are negatively correlated, similar to secondary, diagenetic LMC. Element mapping for Sr and Mg in the primary LMC lithologies revealed no evidence of conversion from aragonite or HMC to LMC, and a homogenous distribution of Mn is in accordance with the absence of late diagenetic alteration. Our results confirm that Sr/Ca ratios, Mg/Ca ratios, and element systematics of primary LMC are indeed distinguishable from diagenetically altered carbonates, enabling the utilization of element geochemistry in recognizing primary signals in carbonate archives.

Keywords: low-magnesium calcite; authigenic carbonates; diagenesis; element contents; Gulf of Mexico

1. Introduction

Carbonate minerals are an important archive of fluid composition, material sources, and environmental conditions, and are widely used in paleoceanography and paleoecology (e.g., [1–3]). Marine authigenic carbonate minerals include dolomite, proto-dolomite, high-magnesium calcite (HMC), low-magnesium calcite (LMC: <5 mol% MgCO₃), and aragonite [4–6]. Aragonite and HMC are metastable and convert into dolomite and LMC in the course of burial [1,7]. During late diagenesis, element contents and isotope compositions of carbonates can be altered (e.g., [6,8–10]). The compositions of original aragonite and HMC lithologies can record either primary, depositional, or secondary

diagenetic processes [11], and cannot typically be used as unaffected archives of the environments where the minerals formed in the first place after the lithologies have been diagenetically altered. By contrast, primary authigenic LMC is a stable archive of pristine geochemical signals. For example, fluid inclusions in marine LMC cement have been used to document the chemical characteristics of the so-called “Calcite Sea” mode of seawater, which resulted in the recognition of changes in the chemical composition of seawater in the Phanerozoic [7]. Consequently, distinguishing primary from secondary, diagenetic LMC is the premise for using this mineral as geological archive [1,7,12–14].

In today’s Aragonite Sea (Mg/Ca mole ratio of seawater ~5.2; [15]), primary authigenic carbonate minerals are commonly either aragonite or HMC (e.g., [16–19]), while primary LMC has only been recognized in some deep-sea environments [20]. Interestingly, authigenic LMC from the seafloor of the Mediterranean Sea and the Gulf of Mexico has been suggested to be of a primary origin, with its formation favored by brine fluids with low Mg/Ca ratios [12–14,16]. Naehr et al. [21] suggested that LMC from Monterey Bay with negative $\delta^{18}\text{O}$ values formed under the influence of meteoric water, either as primary precipitate or through recrystallization. Secondary LMC formed by diagenetic alteration has also been occasionally recognized on the seafloor of the modern Aragonite Sea (e.g., [22,23]). Consequently, constraints on a primary origin of LMC are the prerequisite for using this mineral in the reconstruction of fluid compositions and paleoenvironmental conditions.

Criteria to identify a primary origin of LMC include textures and geochemical characteristics (e.g., [1,24–27]). Although the calcium carbonate mineral lattice changes during diagenetic alteration, the original crystal morphology can be partially retained [22,23,28,29]. Consequently, pseudomorphs and relict textures are common in secondary, diagenetically altered carbonate minerals. For instance, Sandberg [1] assessed the reliability of primary LMC according to the absence of neomorphic textures, indicating diagenetic alteration, and trace element contents. Carbonate crystals formed through recrystallization commonly show other crystal habits, such as blocky mosaics, and tend to be larger [1,30].

According to petrological observations, Huang et al. [13,14] argued that authigenic LMCs from five sites on the seafloor of the northern Gulf of Mexico (GoM) are of primary origin. The GoM deposits are consistent with a formation from fluids with low Mg/Ca ratios, reflecting brine seeps and nearby salt deposits. However, diagenetically altered carbonate is not always easily distinguished from primary authigenic carbonate through petrography alone. In addition to petrography, trends in trace element contents can be used to recognize transformation of aragonite or HMC to LMC (e.g., [6,31,32]). Covariations of the contents of elements such as Sr, Mn, and Mg have been found to help identify the degree of diagenetic alteration (e.g., [6,10,32]). Similarly, back-scattered electron (BSE) imaging has been used to study the process of replacement of aragonite by calcite at hydrothermal vents [33]. Electron microprobe analysis and particle-induced X-ray emission analysis can be used to describe the fate of trace elements during speleothem diagenesis [27].

In order to further constrain the applicability of element compositions for recognizing a primary origin of LMC, element contents of LMC from the northern GoM (sites GC53 and AC601) and highly spatially resolved element distributions were investigated. Reliable recognition of primary signatures in LMC will allow this mineral to be used in the reconstruction of paleoenvironments.

2. Geological Setting

The Gulf of Mexico (GoM) formed during Triassic to Early Cretaceous times when the crust was stretched between the Yucatan microplate and the North American plate [34]. Extensive evaporites were deposited during the rifting. Later on, thick sedimentary strata made of terrigenous sediments accumulated in the northern GoM [35,36]. Widespread salt diapirism generated migration pathways for fluids, favoring hydrocarbon migration [37]. Locally, biogeochemical processes resulting from the mixing of seawater and hydrocarbon-rich seep fluids led to the precipitation of carbonate minerals close to the seafloor [36,38].

Carbonate lithologies dominated by LMC were recovered from the GoM [12–14,39]. It has been suggested that LMC precipitation was favored by the presence of brine seeps [12–14], since the local fluids have low Mg/Ca ratios [40,41]. Study site GC53 overlies a salt diapir and a structural trap of crude oil at the edge of the continental shelf (Figure 1; [42]). Faults, mud volcanos, brine, and hydrocarbon seeps were discovered close to the site [36]. The presence of abundant authigenic carbonates and microbial mats at this site were ascribed to hydrocarbon seepage [36]. Study site AC601 is a brine-charged environment located at the lower edge of the continental slope. A brine pool and brine seeps occur at the seafloor. Dive observations revealed that barite chimneys, carbonate crusts, living mussels, and bacterial mats are scattered on the seafloor [18,19,43].

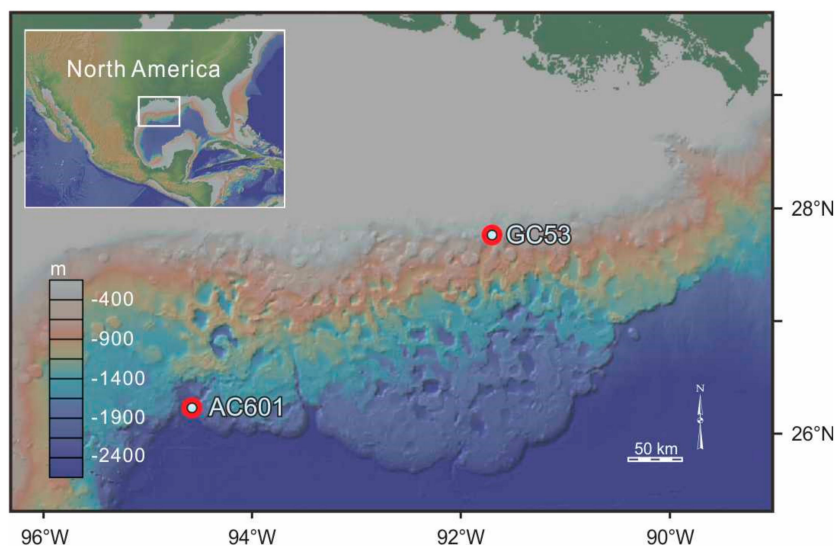


Figure 1. Location of sites GC53 and AC601 in the northern Gulf of Mexico.

3. Materials and Methods

Two types of LMC from the GoM were recognized in previous studies ([13,14]). One sample of each type was selected for this study (Figure 2). Sample D1S2 was recovered during 89-1 dive (1989) of *Pisces II* research submersible targeting site GC53 (water depth of 89 m). The carbonate reveals $\delta^{13}\text{C}$ values between -0.1‰ and 2.0‰ , reflecting precipitation from hydrocarbon-free brine fluids [13]. Sample 4193 was recovered during 4193 dive (2006) of *Alvin* research submersible targeting site AC601 (water depth of 2340 m). The carbonate shows mostly negative $\delta^{13}\text{C}$ values between -9.9‰ and 0.1‰ , interpreted to reflect the effect of mixing of variable carbon sources that include ^{13}C -depleted methane, biodegraded crude oil, seawater-dissolved inorganic carbon, and residual carbon dioxide after the pore water pool was affected by methanogenesis [14]. It was suggested that sample 4193 precipitated from seepage of hydrocarbon-rich brine fluids [14]. The mineralogical compositions of the studied carbonates have been described in detail elsewhere ([13,14]; see also Table 1).

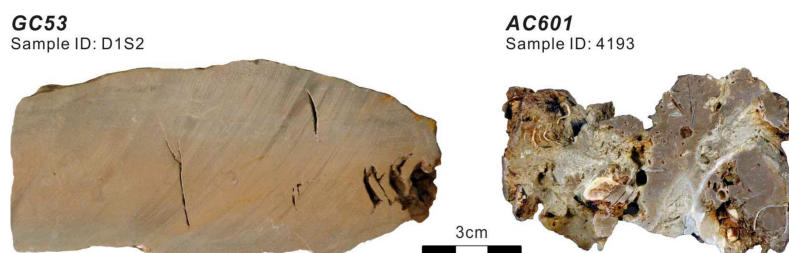


Figure 2. Studied carbonates. Sample D1S2 from site GC53 is an aphanitic micrite. Sample 4193 from site AC601 is characterized by abundant micropores and shell material.

Table 1. Mineral compositions (X-ray diffraction analyses) of low-magnesium calcite lithologies in % and mol% MgCO₃ in low-Mg calcite (right column) from the Gulf of Mexico.

| Site | Sample ID | Quartz | Barite | Siderite | Low-Mg calcite | MgCO ₃ (%) |
|-------|-----------|--------|--------|----------|----------------|-----------------------|
| GC53 | D1S2 * | 5 | | 37 | 58 | 5 |
| AC601 | 4193 ** | 11 | 11 | | 78 | 5 |

MgCO₃ (%) = mol% MgCO₃ in low-Mg calcite. *data from Huang et al. [13]. **data from Huang et al. [14].

Carbonate powders were dissolved for element analyses using either of the two following different methods at the Institute of Geochemistry, Chinese Academy of Sciences. (1) About 20 mg of carbonate powder was treated with a 5% ultra-pure acetic acid for about 2 h to separate carbonate and residue phases. The solution was centrifuged immediately after carbonate dissolution, and then dried on a hotplate. Finally, the samples were dissolved in 3% HNO₃, and spiked with an internal Rh standard (200 ppb) for manganese and strontium contents of carbonate phases. The element compositions of the samples were determined using a Plasma Quant MS ICP–MS. (2) About 50 mg hand-drilled powder was dissolved in HF–HNO₃ solutions in Teflon beakers for measurement of calcium, magnesium, and iron contents of bulk samples. The sealed beakers were placed in an electric oven and kept at 185 °C for about 24 h. Then the solutions were dried in the beakers on a hotplate and redissolved by adding 2 mL ultra-pure HNO₃ and 4 mL deionized water. The beakers were sealed and then kept in an electric oven at 135 °C for 5 h after the solution was spiked with an internal Cd standard (200 ppm). The solution was diluted and then analyzed using a Varian Vista Pro ICP–AES. The accuracy obtained by determining several reference standards (GSR-3, GSD-4, GSD-6, OU-6, and GSR-12 for CaO, MgO, and Fe₂O₃; OU-6, AMH-1, and GBPG-1 for Mn and Sr) was better than 5%.

Element distribution and element spot analyses on thin sections were conducted on a JEOL-8100 electron probe microanalyzer at the Third Institute of Oceanography, Ministry of Natural Resources, China, with which also back-scattered electron images were made. Thin sections were coated with carbon before analysis. Spot analyses and element distributions scanning were carried out at an accelerating voltage of 15 kV and 5 nA.

4. Results

4.1. Element Contents of Carbonate Phases and Bulk Samples

The element contents of the carbonate phases and bulk samples are listed in Table 2. Calcium contents of sample D1S2 vary widely from 23.4% to 41.6% (average: 33.3% ± 6.0%), while sample 4193 shows little variation in calcium contents (45.0% to 48.6%; average: 46.6% ± 1.1%). Both samples show low magnesium contents, ranging from 1.28% to 3.61% (average: 2.11% ± 0.87%) for sample D1S2 and from 1.58% to 2.42% (average: 1.79% ± 0.27%) for sample 4193. Strontium contents of the carbonate phase vary from 153 to 257 µg/g (average: 223 ± 32 µg/g) in sample D1S2, much lower than those of sample 4193 (993 to 1530 µg/g; average: 1217 ± 159 µg/g). Manganese contents of the carbonate phase range from 355 to 539 µg/g (average: 452 ± 63 µg/g) in sample D1S2, and from 1454 to 2993 µg/g (average: 2282 ± 429 µg/g) in sample 4193.

Table 2. Element contents of the studied carbonates.

| Sample No. | CaO | MgO | Fe ₂ O ₃ -T% | Sr | Mn | Sr/Mn | Sr/Ca | Mn/Ca | Mg/Ca |
|------------|------|------|------------------------------------|------|------|-------|----------|----------|-------|
| | % | % | % | µg/g | µg/g | µg/g | mmol/mol | mmol/mol | |
| D1S2-1 | 29.1 | 2.85 | 18.1 | 199 | 539 | 0.37 | 0.44 | 1.89 | 137 |
| D1S2-2 | 23.4 | 3.61 | 25.0 | 153 | 441 | 0.35 | 0.42 | 1.92 | 216 |
| D1S2-3 | 24.9 | 3.41 | 23.7 | 211 | 512 | 0.41 | 0.54 | 2.10 | 192 |
| D1S2-4 | 34.3 | 1.91 | 9.48 | 242 | 462 | 0.52 | 0.45 | 1.37 | 78 |
| D1S2-5 | 38.0 | 1.66 | 7.81 | 256 | 396 | 0.65 | 0.43 | 1.06 | 61 |
| D1S2-6 | 41.6 | 1.28 | 5.11 | 257 | 369 | 0.70 | 0.39 | 0.90 | 43 |

Table 2. Cont.

| Sample No. | CaO | MgO | Fe ₂ O ₃ -T% | Sr | Mn | Sr/Mn | Sr/Ca | Mn/Ca | Mg/Ca |
|------------|------|------|------------------------------------|------|------|-------|----------|----------|-------|
| | % | % | % | µg/g | µg/g | µg/g | mmol/mol | mmol/mol | |
| D1S2-7 | 34.2 | 1.49 | 5.39 | 205 | 515 | 0.40 | 0.38 | 1.53 | 61 |
| D1S2-8 | 35.7 | 1.37 | 4.69 | 236 | 483 | 0.49 | 0.42 | 1.38 | 54 |
| D1S2-9 | 38.9 | 1.38 | 4.75 | 248 | 355 | 0.70 | 0.41 | 0.93 | 50 |
| Average | 33.3 | 2.11 | 11.6 | 223 | 452 | 0.51 | 0.43 | 1.45 | 99 |
| Std Dev | 6.0 | 0.87 | 7.90 | 32 | 63 | 0.13 | 0.04 | 0.42 | 62 |
| 4193-1 | 45.7 | 1.58 | 0.86 | 1380 | 1926 | 0.72 | 1.92 | 4.29 | 48 |
| 4193-2 | 47.5 | 1.60 | 0.83 | 1530 | 2176 | 0.70 | 2.05 | 4.67 | 47 |
| 4193-3 | 46.3 | 2.42 | 1.20 | 1200 | 1454 | 0.83 | 1.65 | 3.20 | 73 |
| 4193-4 | 47.7 | 1.79 | 0.83 | 1150 | 2778 | 0.41 | 1.53 | 5.92 | 53 |
| 4193-5 | 46.6 | 1.62 | 0.91 | 1100 | 2388 | 0.46 | 1.50 | 5.21 | 49 |
| 4193-6 | 46.7 | 1.70 | 1.13 | 993 | 2472 | 0.40 | 1.35 | 5.39 | 51 |
| 4193-7 | 45.6 | 2.08 | 0.99 | 1050 | 2260 | 0.46 | 1.47 | 5.05 | 64 |
| 4193-8 | 48.6 | 1.70 | 0.69 | 1290 | 2993 | 0.43 | 1.69 | 6.27 | 49 |
| 4193-9 | 45.0 | 1.58 | 0.71 | 1260 | 2096 | 0.60 | 1.78 | 4.74 | 49 |
| Average | 46.6 | 1.79 | 0.90 | 1217 | 2283 | 0.56 | 1.66 | 4.97 | 54 |
| Std Dev | 1.1 | 0.27 | 0.17 | 159 | 429 | 0.15 | 0.21 | 0.85 | 8 |

Std Dev = Standard Deviation. Fe₂O₃-T% is total iron as Fe₂O₃.

4.2. Element Distribution in Carbonates

Spot analyses with an electron microprobe helped identify accessory minerals, such as pyrite in sample D1S2 and barite in sample 4193, which coincides with high sulfur contents (Table S1). Spot analyses also revealed variable Fe contents in sample D1S2, reflecting a scattered distribution of siderite. BSE images and element maps are shown in Figures 3 and 4. Manganese and Sr contents are homogeneous in both carbonates (Figure 3B,C and Figure 4B,C), which is consistent with the results obtained by spot analysis. Pyrite and barite, appearing light in BSE images, can be easily discerned (Figures 3A and 4A), with barite revealing high Sr contents (Figures 3B and 4B). In contrast to the homogeneous distribution of Mg in the micrite of sample D1S2, LMC microspar shows higher Mg content than micrite.

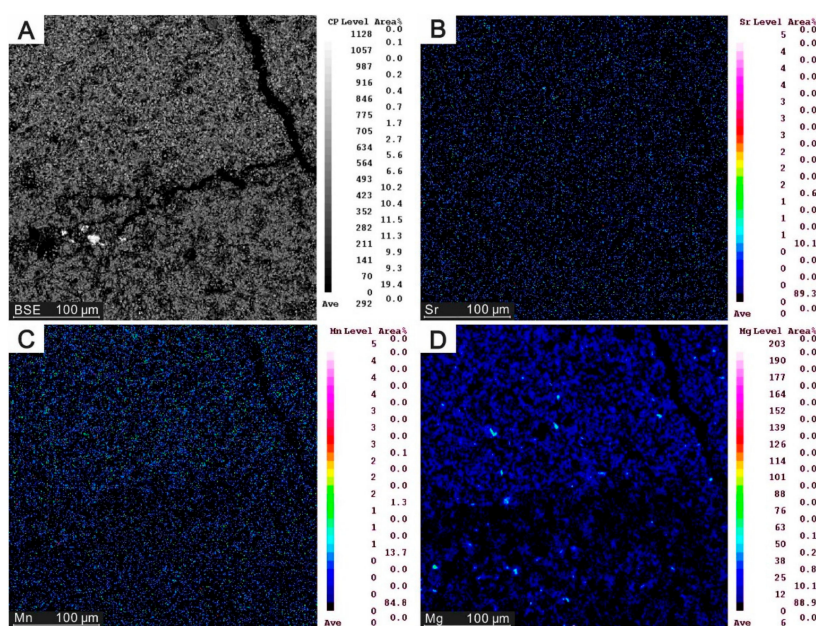


Figure 3. Back-scattered electron (BSE) image (A) and electron microprobe element maps (B–D) of a selected area of D1S2 carbonate, revealing homogeneous distribution of Sr, Mn, and Mg.

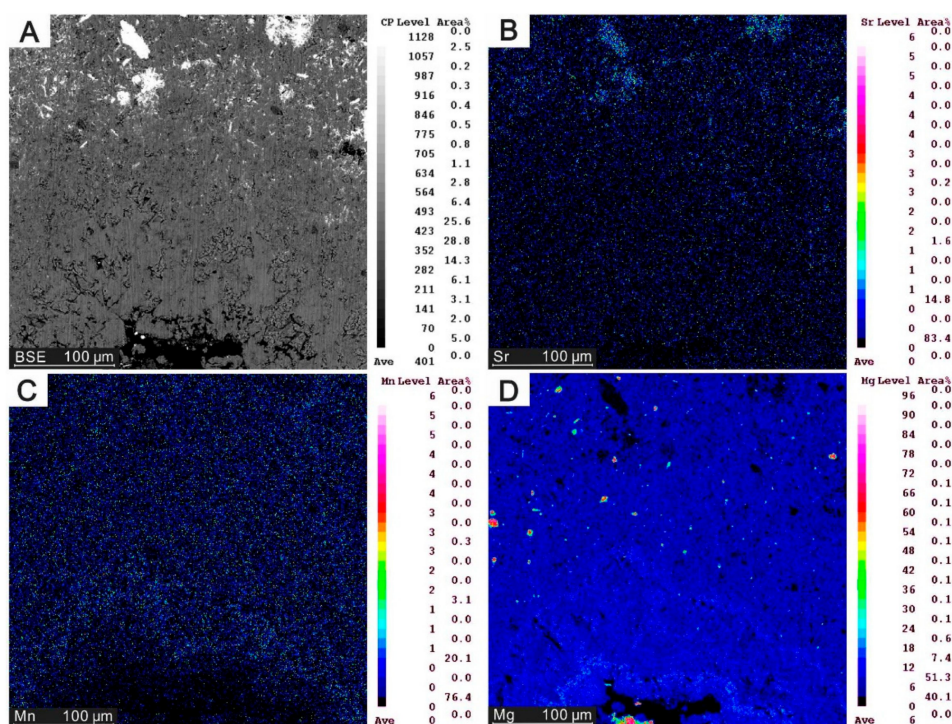


Figure 4. Back-scattered electron (BSE) image (A) and electron microprobe element maps (B–D) of a selected area in 4193 carbonate. The microcrystals in 4193 carbonate are composed of barite and low-magnesium calcite, while the sparry rim is dominated by low-magnesium calcite (A). Strontium and Mn contents are uniform in calcite and strontium contents are higher in barite (B, C); Magnesium contents in the sparry rim are higher than that of micrite (D).

5. Discussion

5.1. Geochemical Features of Primary LMC

Aragonite is orthorhombic and tends to incorporate larger cations (e.g., Sr, Ba, U), while calcite is rhombohedral and accommodates smaller cations (e.g., Mg, Mn; [44,45]). Hence, aragonite cement typically yields significantly higher Sr and lower Mg contents than calcite (e.g., [44,46]). However, secondary calcite resulting from aragonite recrystallization typically retains relatively high Sr contents from its precursor [1,31], still yielding high Sr contents up to thousands of micrograms per gram [47,48]. Consequently, high Sr contents, sometimes in conjunction with low Mg, Fe, and Mn contents, have been used to identify secondary calcite replacing aragonite [1,6,10,46]. Strontium/Ca ratios of the studied GoM LMCs are similar or lower than those of bioskeletal calcite and primary authigenic HMC (~1.36 mmol/mol; [6,49]). The ratios of GoM LMC are much lower than those of authigenic aragonite (~12.3 mmol/mol; [49]), reflecting a potential difference of Sr/Ca ratios between primary LMC and calcite deriving from aragonite recrystallization (e.g., [31,47,48]). Magnesium contents have been reported to increase during the transformation of aragonite to LMC [46]. However, Sr/Ca and Mg/Ca ratios of the studied LMCs reveal no correlation (Figure 5). Taken together, the Sr and Mg compositions of GoM LMCs are much unlike those of LMC resulting from aragonite conversion.

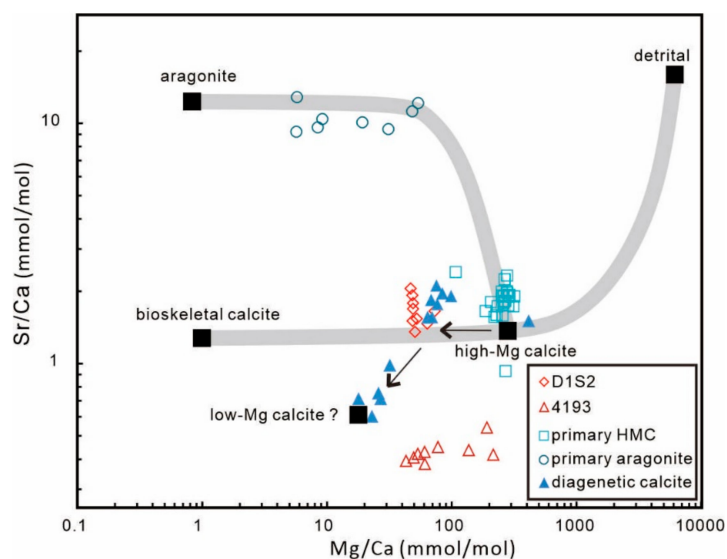


Figure 5. Plot of Sr/Ca vs. Mg/Ca ratios of the studied low-magnesium calcites, primary aragonite, primary high-magnesium calcite (HMC), and diagenetically altered calcite (diagenetic calcite; [6]). The endmembers (filled squares) and mineralogical trends of carbonate minerals are after Bayon et al. [49] and Joseph et al. [6]. Arrows represent the trend of HMC conversion to LMC [6]. Note that the ‘detrital’ represents the endmember of detrital fractions [49].

Partition coefficients of Sr and Mn for LMC are not much different from those for HMC. Consequently, the signal of original HMC could be difficult to recognize in calcite resulting from the conversion of HMC. Diagenetic fluids tend to be rich in Mn and depleted in Sr compared to seawater (e.g., [50–52]). The element concentrations of early diagenetic fluids can be recorded in secondary carbonate when its primary geochemistry is retained to some extent. Joseph et al. [6] studied primary and secondary signatures of ancient seep carbonates and showed that Sr/Ca ratios of calcite are decreasing as Mg/Ca ratios are decreasing (Figure 5); the latter suggesting conversion of HMC to LMC. Along with the conversion of HMC to intermediate-Mg calcite (IMC, 5–12 mol% Mg) and with time to LMC, Sr contents decrease when Mg contents decrease; the corresponding Sr/Ca and Mg/Ca ratios of IMC and LMC show a corresponding covariation [6]. By contrast, the GoM LMCs reveal no such covariation.

Mucci and Morse [53] illustrated that the distribution coefficient of Sr between calcite and solution is dependent on the MgCO_3 content of calcite, proportional to the mole fraction of Mg in calcite. Our results suggest that correlation between Sr/Ca and Mg/Ca is distinguishable between secondary, diagenetically altered LMC, and primary LMC. The Sr and Mn contents of marine carbonates have commonly been used to identify the degree of diagenetic alteration (Figure 6; [32,50,54]). However, authigenic minerals forming at methane seeps have mostly higher Mn contents and lower Sr/Mn than carbonate minerals considered to have retained original seawater signatures (Figure 6; [10]). The primary GoM LMCs reveal similar Sr/Mn ratios and Mn contents like seep carbonates (cf. [6]). We suggest that Sr/Mn ratios and Mn contents of hydrocarbon-seep carbonates, like sample 4193 from site AC601, reflect primary mineralogy, the composition of seep fluids, or the degree of diagenesis. The application of these element systematics for the assessment of the degree of diagenesis is consequently problematic in the case of seep carbonates, unless other constraints on the primary composition of carbonate minerals are available.

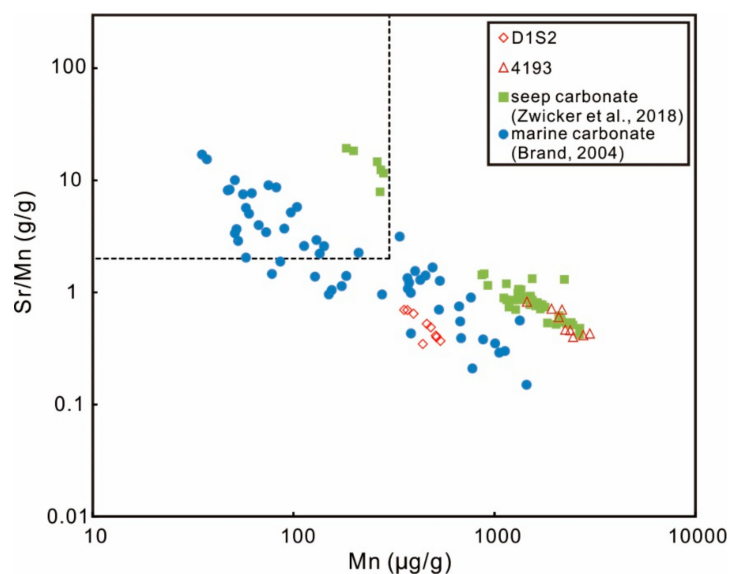


Figure 6. Plot of Mn/Sr ratio vs. Mn content of the primary low-magnesium calcite (LMC; open symbols) in this study and other carbonates used for comparison (filled symbols). It is suggested that carbonates with ≥ 2.0 Sr/Mn and < 300 $\mu\text{g/g}$ Mn (dashed line) retain Sr isotopes of original seawater [55]. The primary LMC reveal low Mn/Sr ratios and relative high Mn contents, which are not distinguishable from the diagenetically altered carbonate.

To sum up, primary LMC can be distinguished from diagenetically altered LMC using Sr, Mn, and Mg contents. However, it needs to be stressed that Sr, Mn, and Mg contents of seep carbonates vary widely. Due to the pervasive fluid mixing during carbonate precipitation at seeps, it can be expected that some primary seep carbonates reveal similar covariation patterns like diagenetically altered carbonate minerals.

5.2. Element Mapping of Carbonates

Segments with primary HMC and aragonite composition can be retained in secondary, diagenetically altered carbonates [6,27,29], showing original geochemical characteristics. Electron microprobe analysis, which allows detailed characterization of element distribution in primary carbonate phases, was used to constrain the degree of alteration of GoM LMCs. For instance, Domínguez-Villar et al. [27] identified residual aragonite with high Sr content in diagenetically altered carbonate through element microanalyses. Distributions of Mn, Sr, and Mg in discrete textures have been mapped in diagenetically altered seep carbonates using laser ablation inductively coupled mass spectrometry [6], revealing significant differences between primary HMC and crystals resulting from recrystallization; these observations were consistent with cathodoluminescence patterns [6]. GoM sample D1S2 is dominated by LMC with a homogenous micritic texture. The lithology reveals a homogeneous distribution of Sr and Mg, agreeing with the absence of aragonite or HMC conversion to LMC. Similarly, the homogeneous distribution of Mn suggests the absence of alteration caused by late-stage diagenetic fluids. GoM sample 4193 is characterized by a matrix of clotted micrite and an isopachous rim of microspar. Microspar precipitated in pores and fractures after clotted micrite had formed. The contents of Sr and Mn are not distinguishable between microspar and clotted micrite, indicating similar pore fluid composition. Interestingly, the Mg content of the later-stage microspar is even slightly higher than that of the micritic matrix, opposite to late diagenetic microspar that typically shows lower Mg contents than primary micrite [6]. Since the studied LMCs have been suggested to have formed from brine fluids with low Mg/Ca ratio [13,14], relatively higher Mg contents of microspar could reflect a higher Mg concentration of pore fluids due to increased seawater ingress during the precipitation of microspar. To sum up, mapping revealed that the element distribution within GoM

carbonates is dominated by primary LMC and is different from distributions within diagenetically altered carbonates.

6. Conclusions

This study investigates element distribution within primary LMC deposits recovered from the seafloor of the Gulf of Mexico (GoM) to provide a perspective for distinguishing primary low-Mg calcite (LMC) from diagenetically altered LMC minerals. Strontium/Ca ratios of the GoM LMCs are close to or lower than those of primary HMC, and no covariation with Mg contents is apparent. The encountered element compositions are unlike those expected in the case of conversion of aragonite or high-Mg calcite (HMC) to LMC. However, similar to some diagenetically altered carbonates, the studied LMC lithologies show a negative correlation between Sr/Mn ratios and Mn contents. Such inhomogeneous composition of the samples can be explained by fluid mixing during carbonate precipitation in the dynamic subseafloor environments in seep settings of the GoM. Nonetheless, Sr, Mg, and Mn distributions obtained by electron microprobe analysis reveal no evidence of conversion of aragonite or HMC to LMC, in sharp contrast with the compositions of diagenetically altered, secondary calcites. The element compositions of the primary GoM LMCs, formed at times of a modern Aragonite Sea, are distinguishable from secondary, diagenetic calcite. This can be applied to recognize primary LMCs in the rock record, and provides a basis for the reconstruction of environmental conditions during carbonate precipitation in the geological past.

Supplementary Materials: The following files are available online at <http://www.mdpi.com/2075-163X/10/4/299/s1>, Figure S1. Thin section (A-D; plane polarized light) and scanning electron microscopy (E and F) photomicrographs of carbonates, Table S1: Element contents (wt %) revealed by point analyses in low-Magnesium calcite.

Author Contributions: Conceptualization, D.F. and H.H.; methodology, H.H.; formal analysis, H.H., X.W., S.G. and N.K.; investigation, H.H.; resources, H.H.; data curation, H.H.; writing—Original draft preparation, H.H., X.W., S.G., D.B., J.P., D.C. and D.F.; writing—Review and editing, H.H., X.W., S.G., D.B., J.P. and D.F.; visualization, H.H.; supervision, D.F.; project administration, D.F.; funding acquisition, D.F. All authors have read and agreed to the published version of the manuscript.

Funding: This study was supported by the NSF of China (Grants: 41761134084, 41773091, 41730528, and 41676046) and the Deutsche Forschungsgemeinschaft (PE 847/7-1).

Acknowledgments: We thank Prof. Harry H. Roberts (LSU) for providing the samples. Samples were collected during projects funded by the U.S. Bureau of Ocean Energy Management and the National Oceanic and Atmospheric Administration's National Undersea Research Program. Y.D. Sun (SCSIO, CAS) and Y.B. Peng (LSU) are thanked for the help with analyses. We thank the editor and two anonymous reviewers for their comments.

Conflicts of Interest: The authors declare that they have no conflicts of interest regarding the publication of this paper.

References

1. Sandberg, P.A. An oscillating trend in Phanerozoic non-skeletal carbonate mineralogy. *Nature* **1983**, *305*, 19–22. [[CrossRef](#)]
2. Farkaš, J.; Böhm, F.; Wallmann, K.; Blenkinsop, J.; Eisenhauer, A.; van Geldern, R.; Munnecke, A.; Voigt, S.; Veizer, J. Calcium isotope record of Phanerozoic oceans: Implications for chemical evolution of seawater and its causative mechanisms. *Geochim. Cosmochim. Acta* **2007**, *71*, 5117–5134. [[CrossRef](#)]
3. Tong, H.; Feng, D.; Cheng, H.; Yang, S.; Wang, H.; Min, A.G.; Edwards, R.L.; Chen, Z.; Chen, D. Authigenic carbonates from seeps on the northern continental slope of the South China Sea: New insights into fluid sources and geochronology. *Mar. Pet. Geol.* **2013**, *43*, 260–271. [[CrossRef](#)]
4. Baker, P.A.; Kastner, M. Constraints on the formation of sedimentary dolomite. *Science* **1981**, *213*, 214–216. [[CrossRef](#)] [[PubMed](#)]
5. Peckmann, J.; Reimer, A.; Luth, U.; Luth, C.; Hansen, B.T.; Heinicke, C.; Hoefs, J.; Reitner, J. Methane-derived carbonates and authigenic pyrite from the northwestern Black Sea. *Mar. Geol.* **2001**, *177*, 129–150. [[CrossRef](#)]
6. Joseph, C.; Campbell, K.A.; Torres, M.E.; Martin, R.A.; Pohlman, J.W.; Riedel, M.; Rose, K. Methane-derived authigenic carbonates from modern and paleoseeps on the Cascadia margin: Mechanisms of formation and diagenetic signals. *Palaeogeogr. Palaeoclimatol. Palaeoecol.* **2013**, *390*, 52–67. [[CrossRef](#)]

7. Johnson, W.J.; Goldstein, R.H. Cambrian sea water preserved as inclusions in marine low-magnesium calcite cement. *Nature* **1993**, *362*, 335–337. [[CrossRef](#)]
8. Tong, H.; Wang, Q.; Peckmann, J.; Cao, Y.; Chen, L.; Zhou, W.; Chen, D. Diagenetic alteration affecting $\delta^{18}\text{O}$, $\delta^{13}\text{C}$ and $^{87}\text{Sr}/^{86}\text{Sr}$ signatures of carbonates: A case study on Cretaceous seep deposits from Yarlung-Zangbo Suture Zone, Tibet, China. *Chem. Geol.* **2016**, *444*, 71–82. [[CrossRef](#)]
9. Kimmig, S.R.; Holmden, C. Multi-proxy geochemical evidence for primary aragonite precipitation in a tropical-shelf ‘calcite sea’ during the Hirnantian glaciation. *Geochim. Cosmochim. Acta* **2017**, *206*, 254–272. [[CrossRef](#)]
10. Zwicker, J.; Smrzka, D.; Himmler, T.; Monien, P.; Gier, S.; Goedert, J.L.; Peckmann, J. Rare earth elements as tracers for microbial activity and early diagenesis: A new perspective from carbonate cements of ancient methane-seep deposits. *Chem. Geol.* **2018**, *501*, 77–85. [[CrossRef](#)]
11. Hood, A.V.S.; Planavsky, N.J.; Wallace, M.W.; Wang, X. The effects of diagenesis on geochemical paleoredox proxies in sedimentary carbonates. *Geochim. Cosmochim. Acta* **2018**, *232*, 265–287. [[CrossRef](#)]
12. Feng, D.; Roberts, H.H.; Joye, S.B.; Heydari, E. Formation of low-magnesium calcite at cold seeps in an aragonite sea. *Terra Nova* **2014**, *26*, 150–156. [[CrossRef](#)]
13. Huang, H.; Gong, S.; Li, N.; Birgel, D.; Peckmann, J.; Jin, M.; Cheng, M.; Roberts, H.H.; Chen, D.; Feng, D. Formation of authigenic low-magnesium calcite from sites SS296 and GC53 of the Gulf of Mexico. *Minerals* **2019**, *9*, 251. [[CrossRef](#)]
14. Huang, H.; Wang, X.; Gong, S.; Krake, N.; Jin, M.; Li, N.; Birgel, D.; Peckmann, J.; Cheng, M.; Roberts, H.H.; et al. New constraints on the formation of hydrocarbon-derived low magnesium calcite at brine seeps in the Gulf of Mexico. *Sediment. Geol.* **2020**, *398*, 105572. [[CrossRef](#)]
15. Hardie, L.A. Secular variation in seawater chemistry: An explanation for the coupled secular variation in the mineralogies of marine limestones and potash evaporites over the past 600 m. *Geology* **1996**, *24*, 279–283. [[CrossRef](#)]
16. Aloisi, G.; Pierre, C.; Rouchy, J.-M.; Foucher, J.-P.; Woodside, J. Methane-Related authigenic carbonates of eastern Mediterranean Sea mud volcanoes and their possible relation to gas hydrate destabilisation. *Earth Planet. Sci. Lett.* **2000**, *184*, 321–338. [[CrossRef](#)]
17. Stanley, S.M.; Ries, J.B.; Hardie, L.A. Low-Magnesium calcite produced by coralline algae in seawater of late cretaceous composition. *Proc. Natl. Acad. Sci. USA* **2002**, *99*, 15323–15326. [[CrossRef](#)]
18. Roberts, H.H.; Shedd, W.; Hunt, J. Dive site geology: DSV ALVIN (2006) and ROV JASON II (2007) dives to the middle-lower continental slope, northern Gulf of Mexico. *Deep Sea Res. Part II* **2010**, *57*, 1837–1858. [[CrossRef](#)]
19. Roberts, H.H.; Feng, D.; Joye, S.B. Cold-seep carbonates of the middle and lower continental slope, northern Gulf of Mexico. *Deep Sea Res. Part II* **2010**, *57*, 2040–2054. [[CrossRef](#)]
20. Longman, M.W. Carbonate diagenetic textures from nearsurface diagenetic environments. *Am. Assoc. Pet. Geol. Bull.* **1980**, *64*, 461–487.
21. Naehr, T.H.; Eichhubl, P.; Orphan, V.J.; Hovland, M.; Paull, C.K.; Ussler, W.; Lorenson, T.D.; Greene, H.G. Authigenic carbonate formation at hydrocarbon seeps in continental margin sediments: A comparative study. *Deep Sea Res. Part II* **2007**, *54*, 1268–1291. [[CrossRef](#)]
22. Gomberg, D.N.; Bonatti, E. High-Magnesian calcite: Leaching of magnesium in the deep sea. *Science* **1970**, *168*, 1451–1453. [[CrossRef](#)]
23. Schlager, W.; James, N.P. Low-Magnesian calcite limestones forming at the deep-sea floor, Tongue of the Ocean, Bahamas. *Sedimentology* **1978**, *25*, 675–702. [[CrossRef](#)]
24. Banner, J.L.; Hanson, G.N. Calculation of simultaneous isotopic and trace element variations during water-rock interaction with applications to carbonate diagenesis. *Geochim. Cosmochim. Acta* **1990**, *54*, 3123–3137. [[CrossRef](#)]
25. Swart, P.K. The geochemistry of carbonate diagenesis: The past, present and future. *Sedimentology* **2015**, *62*, 1233–1304. [[CrossRef](#)]
26. Casella, L.A.; Griesshaber, E.; Yin, X.; Ziegler, A.; Mavromatis, V.; Müller, D.; Ritter, A.C.; Hippler, D.; Harper, E.M.; Dietzel, M.; et al. Experimental diagenesis: Insights into aragonite to calcite transformation of *Arctica islandica* shells by hydrothermal treatment. *Biogeosciences* **2017**, *14*, 1461–1492. [[CrossRef](#)]

27. Domínguez-Villar, D.; Krklec, K.; Pelicon, P.; Fairchild, I.J.; Cheng, H.; Edwards, L.R. Geochemistry of speleothems affected by aragonite to calcite recrystallization—Potential inheritance from the precursor mineral. *Geochim. Cosmochim. Acta* **2017**, *200*, 310–329. [[CrossRef](#)]
28. Budd, D.A. Petrographic products of freshwater diagenesis in Holocene ooid sands, Schooner Cays, Bahamas. *Carbonates Evaporites* **1988**, *3*, 143–163. [[CrossRef](#)]
29. Frank, T.D.; Lohmann, K.C. Diagenesis of fibrous magnesian calcite marine cement: Implications for the interpretation of $\delta^{18}\text{O}$ and $\delta^{13}\text{C}$ values of ancient equivalents. *Geochim. Cosmochim. Acta* **1996**, *60*, 2427–2436. [[CrossRef](#)]
30. Denison, R.E.; Koepnick, R.B.; Burke, W.H.; Hetherington, E.A. Construction of the Cambrian and Ordovician seawater $^{87}\text{Sr}/^{86}\text{Sr}$ curve. *Chem. Geol.* **1998**, *152*, 325–340. [[CrossRef](#)]
31. Beauchamp, B.; Savard, M. Cretaceous chemosynthetic carbonate mounds in the Canadian Arctic. *Palaios* **1992**, *7*, 434–450. [[CrossRef](#)]
32. Brand, U. Carbon, oxygen and strontium isotopes in Paleozoic carbonate components: An evaluation of original seawater-chemistry proxies. *Chem. Geol.* **2004**, *204*, 23–44. [[CrossRef](#)]
33. Perdikouri, C.; Piazzolo, S.; Kasiopas, A.; Schmidt, B.C.; Putnis, A. Hydrothermal replacement of aragonite by calcite: Interplay between replacement, fracturing and growth. *Eur. J. Mineral.* **2013**, *25*, 123–136. [[CrossRef](#)]
34. Salvador, A. Late Triassic-Jurassic paleogeography and origin of Gulf of Mexico basin. *Am. Assoc. Pet. Geol. Bull.* **1987**, *71*, 419–451.
35. Roberts, H.H.; Aharon, P.; Carney, R.; Larkin, J.; Sassen, R. Sea floor responses to hydrocarbon seeps, Louisiana continental slope. *Geo-Mar. Lett.* **1990**, *10*, 232–243. [[CrossRef](#)]
36. Roberts, H.H.; Aharon, P. Hydrocarbon-derived carbonate buildups of the northern Gulf of Mexico continental slope: A review of submersible investigations. *Geo-Mar. Lett.* **1994**, *14*, 135–148. [[CrossRef](#)]
37. Sassen, R.; MacDonald, I.R. Evidence of structure H hydrate, Gulf of Mexico continental slope. *Org. Geochem.* **1994**, *22*, 1029–1032. [[CrossRef](#)]
38. Feng, D.; Chen, D.; Roberts, H.H. Petrographic and geochemical characterization of seep carbonate from Bush Hill (GC 185) gas vent and hydrate site of the Gulf of Mexico. *Mar. Pet. Geol.* **2009**, *26*, 1190–1198. [[CrossRef](#)]
39. Hu, Y.; Feng, D.; Peckmann, J.; Roberts, H.H.; Chen, D. New insights into cerium anomalies and mechanisms of trace metal enrichment in authigenic carbonate from hydrocarbon seeps. *Chem. Geol.* **2014**, *381*, 55–66. [[CrossRef](#)]
40. Aharon, P.; Roberts, H.H.; Snelling, R. Submarine venting of brines in the deep Gulf of Mexico: Observations and geochemistry. *Geology* **1992**, *20*, 483–486. [[CrossRef](#)]
41. Fu, B.; Aharon, P. Sources of hydrocarbon-rich fluids advecting on the seafloor in the Northern Gulf of Mexico. *Gulf Coast Assoc. Geol. Soc. Trans.* **1998**, *82*, 73–82.
42. Cook, D.J.; Donfro, P. Joliet Field thrust fault structure and stratigraphy, Green Canyon Block 184, offshore Louisiana. *Am. Assoc. Pet. Geol. Bull.* **1991**, *41*, 100–121.
43. Brooks, J.M.; Fisher, C.; Roberts, H.; Carney, B.; Macdonald, I.; Cordes, E.; Joye, S.; Goehring, L.; Bernard, B.; Wolff, G. *Investigations of Chemosynthetic Communities on the Lower Continental Slope of the Gulf of Mexico Volume I: Final Report*; U.S. Department of the Interior, Bureau of Ocean Energy Management, Gulf of Mexico OCS Region: New Orleans, LA, USA, 2014.
44. Tucker, M.E.; Wright, V.P. Carbonate Mineralogy and Chemistry. In *Carbonate Sedimentology*; Blackwell Publishing Ltd.: Oxford, UK, 1990; pp. 284–313.
45. Smrzka, D.; Zwicker, J.; Bach, W.; Feng, D.; Himmler, T.; Chen, D.; Peckmann, J. The behavior of trace elements in seawater, sedimentary pore water, and their incorporation into carbonate minerals: A review. *Facies* **2019**, *65*, 41. [[CrossRef](#)]
46. Brand, U. Aragonite-Calcite transformation based on Pennsylvanian molluscs. *Geol. Soc. Am. Bull.* **1989**, *101*, 377–390. [[CrossRef](#)]
47. Buggisch, W.; Krumm, S. Palaeozoic cold seep carbonates from Europe and North Africa—An integrated isotopic and geochemical approach. *Facies* **2005**, *51*, 566–583. [[CrossRef](#)]
48. Peckmann, J.L.; Campbell, K.A.; Walliser, O.H.; Reitner, J. A Late Devonian hydrocarbon-seep deposit dominated by dimerlloid brachiopods, Morocco. *Palaios* **2007**, *22*, 114–122. [[CrossRef](#)]

49. Bayon, G.; Pierre, C.; Etoubleau, J.; Voisset, M.; Cauquil, E.; Marsset, T.; Sultan, N.; Le Drezen, E.; Fouquet, Y. Sr/Ca and Mg/Ca ratios in Niger Delta sediments: Implications for authigenic carbonate genesis in cold seep environments. *Mar. Geol.* **2007**, *241*, 93–109. [[CrossRef](#)]
50. Brand, U.; Veizer, J. Chemical diagenesis of a multicomponent carbonate system; 1, Trace elements. *J. Sediment. Petrol.* **1980**, *50*, 1219–1236.
51. Derry, L.A.; Kaufman, A.J.; Jacobsen, S.B. Sedimentary cycling and environmental change in the Late Proterozoic: Evidence from stable and radiogenic isotopes. *Geochim. Cosmochim. Acta* **1992**, *56*, 1317–1329. [[CrossRef](#)]
52. Edwards, C.T.; Saltzman, M.R.; Leslie, S.A.; Bergström, S.M.; Sedlacek, A.R.C.; Howard, A.; Bauer, J.A.; Sweet, W.C.; Young, S.A. Strontium isotope ($^{87}\text{Sr}/^{86}\text{Sr}$) stratigraphy of Ordovician bulk carbonate: Implications for preservation of primary seawater values. *Geol. Soc. Am. Bull.* **2015**, *127*, 1275–1289. [[CrossRef](#)]
53. Mucci, A.; Morse, J.W. The incorporation of divalent Mg and divalent Sr into calcite overgrowths: Influences of growth rate and solution composition. *Geochim. Cosmochim. Acta* **1983**, *47*, 217–233. [[CrossRef](#)]
54. Jacobsen, S.B.; Kaufman, A.J. The Sr, C and O isotopic evolution of Neoproterozoic seawater. *Chem. Geol.* **1999**, *161*, 37–57. [[CrossRef](#)]
55. Denison, R.E.; Koepnick, R.B.; Fletcher, A.; Howell, M.W.; Callaway, W.S. Criteria for the retention of original seawater $^{87}\text{Sr}/^{86}\text{Sr}$ in ancient shelf limestones. *Chem. Geol.* **1994**, *112*, 131–143. [[CrossRef](#)]



© 2020 by the authors. Licensee MDPI, Basel, Switzerland. This article is an open access article distributed under the terms and conditions of the Creative Commons Attribution (CC BY) license (<http://creativecommons.org/licenses/by/4.0/>).